AN3180
Application note

A 200 W ripple-free input current PFC pre-regulator with the L6563S

Introduction

A major limitation of transition-mode-operated PFC pre-regulators is their considerable input ripple current, which requires a large differential mode (DM) line filter to meet EMI requirements. The ripple-steering technique, with its ability to reduce an inductor ripple current, theoretically to zero, can be very helpful in reducing the need for DM filtering in any offline switching converter and in PFC pre-regulators in particular, where DM noise is an issue as there is no electrolytic capacitor just after the bridge. This application note illustrates the use of this technique, providing both the theoretical base and practical considerations to enable successful implementation. Furthermore, it shows the bench results of the EVL6563S-ZRC200 demonstration board, a 200 W ripple-free PFC pre-regulator based on an L6563S controller, designed according to the criterion proposed in this application note.

Figure 1. EVL6563S-200ZRC 200W PFC demonstration board

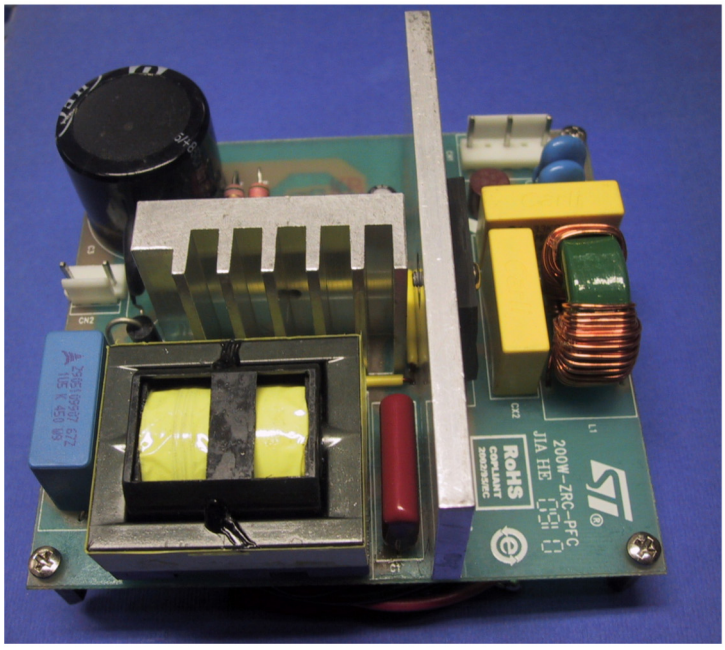

Contents

List of figures

1 Basic topologies with zero-ripple current

Coupled magnetic devices have been around since the early days of electronics, and their application to power switching circuits dates back to the late 70's with the experiments on the Cuk converter, from which “magnetic integration” originated. With this technique, inductors and transformers are combined into a single physical structure to reduce the component count, usually with little or no penalty at all on the converter's characteristics, sometimes even enhancing its operation. During initial experiments on the Cuk converter the zero-ripple current phenomenon was first observed. The technique derived by the use of this phenomenon is known as ripple-steering or ripple cancellation. Besides providing an excellent discussion, also gives an interesting historical outline of the subject (see *References 1*). The application of the zero-ripple current phenomenon is of considerable interest in switching converters, where there are at least two reasons why it is desirable to minimize inductor ripple currents. Firstly, lowering ripple current in inductors reduces the stress on converter capacitors, resulting in either lower associated power loss or more relaxed filtering requirements. Secondly, and often more importantly, most converter topologies have pulsating current at either input or output or both, and most applications require low conducted noise at both ports, because of EMC requirements or load requirements.

Figure 2. Some basic topologies with zero-ripple current characteristics

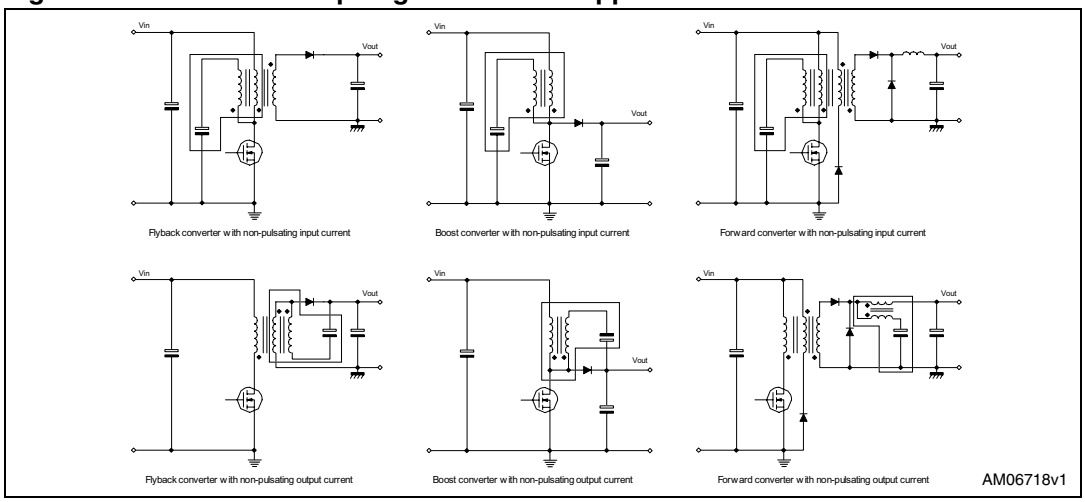

This issue is commonly addressed with the use of additional LC filters, whose impact on both the overall converter size and cost is not at all negligible, not to mention their interaction with the small-signal dynamics which sometimes cause poor dynamic response issues or even stability issues. In particular, in offline converters, where EMC regulations specify limits to the amount of conducted and radiated emissions, a technique like ripple-steering which makes the input current non-pulsating or nearly so, therefore eliminating most of the differential mode conducted noise, is advantageous as it enables the reduction in EMI filter size and complexity, especially in its differential filtering section (Cx capacitors and differential mode inductors).

Reducing Cx capacitors to a minimum brings an additional benefit to applications with tight specifications on standby consumption: Cx capacitors cause a considerable reactive current to flow through the filter, which is a source of additional and unwanted loss (even 0.1 W or more at high line); furthermore, the discharge resistor which, for safety, must be placed in parallel to Cx can be higher. As a result, both losses are minimized.

All converter topologies are capable of producing zero-ripple current phenomenon, provided there are two or more inductors which have equal (or, more generally, proportional) voltages of equal frequency and phase. Some topologies, such as Cuk and SEPIC, have two inductors, which can be coupled on a common magnetic core: so they immediately lend themselves to ripple-steering. The other basic topologies - buck, boost, buck-boost, flyback and single-output forward - have typically a single inductor and then, to reduce its ripple current to zero, they must be modified with the addition of a second winding wound on the same inductor core. Moreover, this additional winding must be connected in such a way as to have the same voltage as the winding where the ripple current is to be cancelled.

Figure 2 shows examples of how to modify some of the basic topologies to achieve zero-ripple inductor current, to have non-pulsating current at either the input or the output. In all examples it is possible to recognize the addition of a cell, a two-port circuit commonly termed a smoothing transformer and shown separately in *Figure 3*. This cell is able to divert, or steer, the AC component (the ripple current) from the externally accessible DC winding, to the AC winding (cancellation winding) whose current conduction path goes directly to the input port, leaving only DC current flowing through the DC winding and the output port. Note that the denomination of input and output ports of the smoothing transformer cell is different from that of input and output of the converter where the cell is applied.

Figure 3. Smoothing transformer and related currents

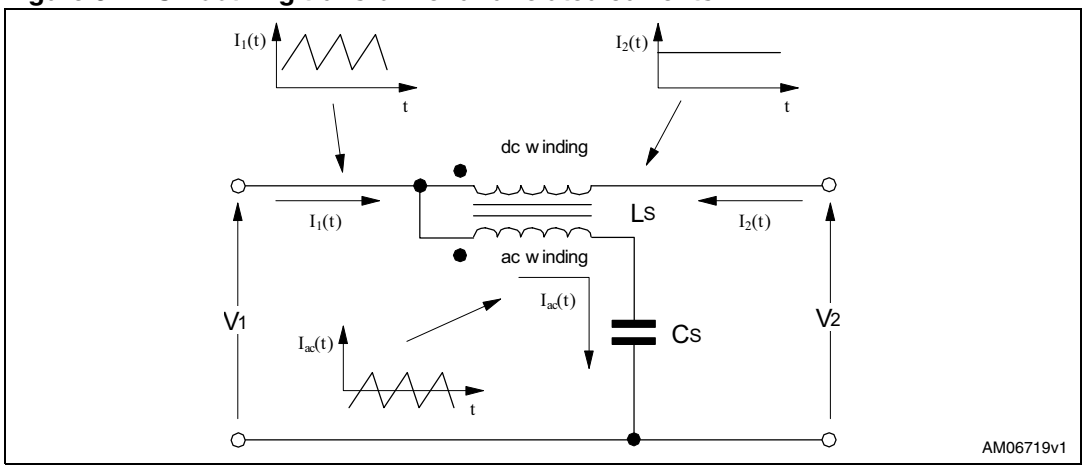

This application note, after reviewing the theoretical base, considers the realization of zero-ripple inductor current to minimize the input ripple in a TM PFC pre-regulator. In these systems, the large input ripple is one of the major limitations to its use at higher power levels.

2 Zero-ripple current phenomenon: theory

Zero-ripple current in one of a two-winding coupled inductor, having self-inductances L1 and L2, can be achieved if the coupling coefficient k, given by:

Equation 1

$$k = \frac{M}{\sqrt{L_1 L_2}}$$

(M is their mutual inductance), and the effective turns ratio n_e defined as:

Equation 2

$$n_e = \sqrt{\frac{L_2}{L_1}}$$

is such that either k n_e = 1 or k = n_e, provided the windings are fed by the same voltage.

To confirm this, it is convenient to consider the a = k n_e coupled-inductor model (refer to *Appendix A*) with the terminals excited by proportional voltages v(t) and αv(t) having the same frequency and phase, shown in *Figure 4*. This is the only condition to be imposed on the terminal voltages, their actual waveform is irrelevant.

Figure 4. Coupled inductor a = k n_e model under zero-ripple current conditions

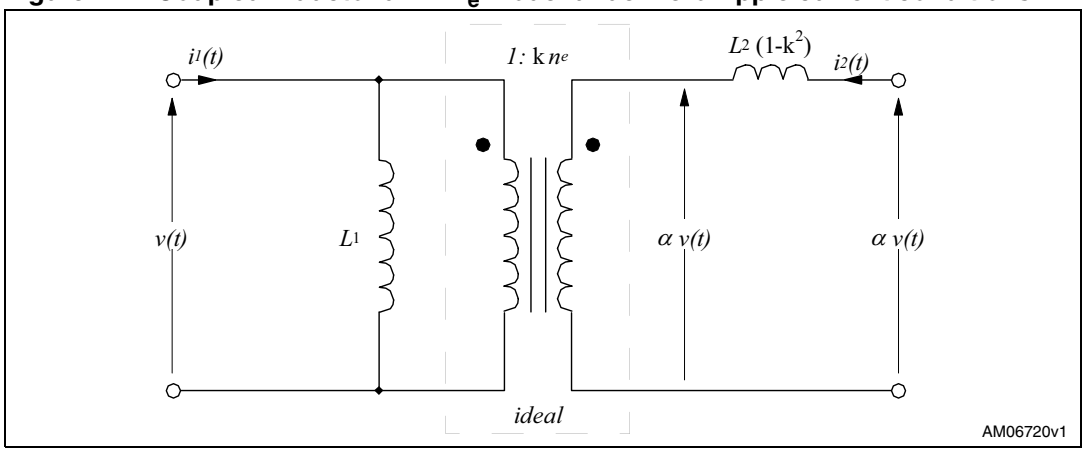

Figure 4 shows that, in order for the secondary ripple current (i.e. $di_2(t)/dt$) to be zero, the voltage across the inductance L_2 (1-k^2) must be zero, that is, the voltage on either side of it must be the same. Thereby:

Equation 3

$$k\,n_e\,v(t) = \alpha\,v(t) \quad \Rightarrow \quad k\,n_e = \alpha$$

Figure 5. Coupled inductor a = n_e/k model under zero-ripple current conditions

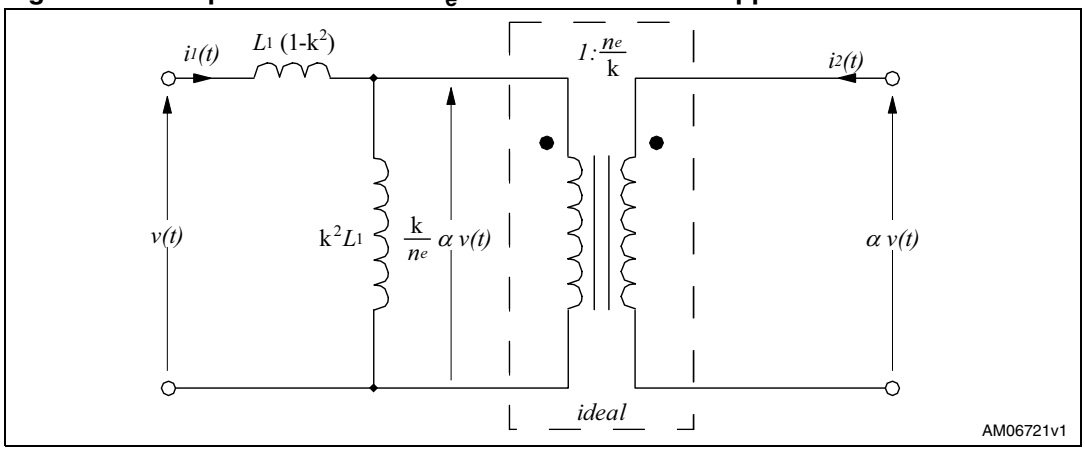

Similarly, considering the model of *Figure 5*, again excited by proportional voltages v(t) and αv(t), it is equally apparent that, in order for the primary ripple current to be zero the voltage across the inductance L_1 (1-k^2) must be zero, that is, the voltage on either side of it must be the same:

Equation 4

$$v(t) = \frac{k}{n_e}\alpha\, v(t) \quad \Rightarrow \quad \frac{k}{n_e}\alpha = 1 \quad \Rightarrow \quad k\,\alpha = n_e$$

If in *Equation 3* and *4* α=1, which means that equal voltages are impressed on either side of the coupled inductor, we find the above mentioned assertion. As α=1 is the most common condition found in switching converters, from now on this is the only case that is taken into consideration, therefore:

- $k\,n_e = 1$ condition for zero-ripple secondary current
- $k = n_e$ condition for zero-ripple primary current

Note that, as k < 1, to obtain a zero-ripple secondary current it must be n_e > 1, that is L_2 > L_1, while to obtain a zero-ripple primary current it must be n_e < 1, that is L_1 > L_2; and so ripple current cannot be reduced to zero in both windings simultaneously. In *Figure 4* and *5*, note also that the inductance of the winding, where zero-ripple current is achieved, is irrelevant, since there is no ripple current flowing (only DC current can flow). As a consequence, the zero-ripple current winding reflects an open circuit to the other one, so that the inductance seen at the terminals of that winding equals exactly its self-inductance.

The designation of which winding is the primary or the secondary is purely conventional. Therefore, we consider only one zero-ripple current condition and arbitrarily assume the condition to be assigned to the secondary winding:

Equation 5

$$k\,n_e = 1$$

which, consistent with the terminology used for the smoothing transformer of *Figure 3*, is termed DC winding, while the primary winding is termed AC or cancellation winding. *Equation 5*, considering *Equation 1* and *2* can be written in different equivalent ways:

Equation 6

$$k\,n_e = k\sqrt{\frac{L_2}{L_1}} = \frac{M}{L_1} = 1$$

Equation 5 and *6* are noteworthy because of their concision in expressing the conditions for zero-ripple current phenomenon to occur, but unfortunately its physical nature is not shown. To provide some physical insight, let us consider the a = *n* coupled inductor model (n is the physical turn ratio N_2/N_1) excited by equal terminal voltages v(t), shown in *Figure 6*.

Figure 6. Coupled inductor a = *n* model under zero-ripple current conditions

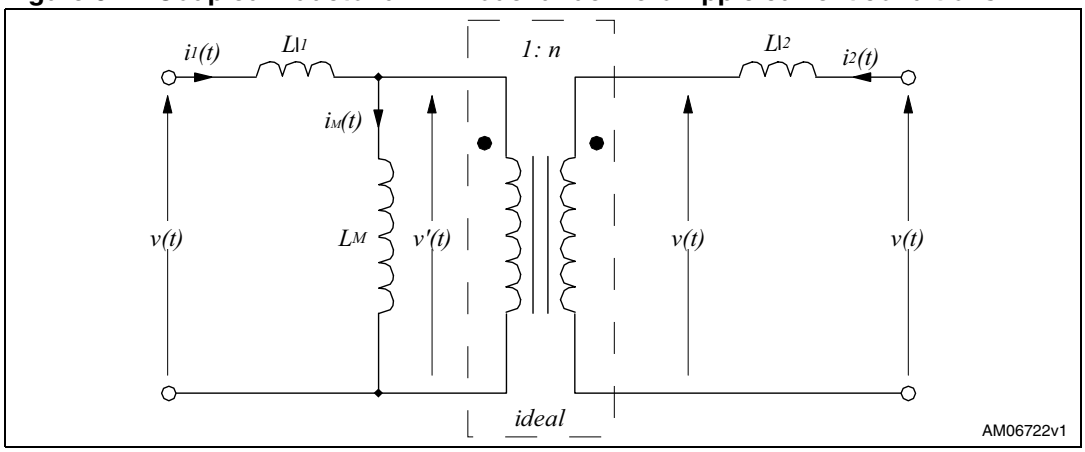

Proceeding with the same technique, in order for the ripple current $i_2(t)$ to be zero, the voltage across the secondary leakage L_{l2} must be zero, that is, the voltages on either side of L_{l2} must be equal to one another. On the other hand, if i2(t)=0 the voltage impressed on the primary side of the ideal transformer v'(t) is given by the ratio of the inductive divider made up of the primary leakage inductance L_{l1} and the magnetizing inductance L_M; the voltage applied to the left-hand side of L_{l2} is equal to $nv'(t)$. Then, there is zero-ripple current on the secondary side of the coupled inductor if the following condition is fulfilled:

Equation 7

$$\frac{L_M}{L_{\ell 1} + L_M} n\,v(t) = v(t) \quad \Rightarrow \quad \frac{L_M}{L_{\ell 1} + L_M} n = \frac{L_M}{L_1} n = 1$$

which is equivalent to *Equation 5* and *6*, as can be easily shown, considering that $L_M = M/n$.

Equation 7 provides the desired physical interpretation of the zero-ripple current condition: it occurs when the turn ratio exactly compensates for the primary winding leakage flux, so that the primary winding induces, by transformer effect, a voltage identical to its own excitation voltage on the secondary winding; and so, if this is externally excited by the same voltage, no ripple current flows through it.

The extensions of this interpretation to the case of zero-ripple primary current (just reflect the magnetizing inductance L_M to the secondary side) and to that of proportional excitation voltages ($\alpha \neq 1$) are obvious.

To summarize the main results of this brief analysis:

1. Ripple-current can be reduced to zero in either winding of a two-winding coupled inductor, but not simultaneously
2. The only conditions imposed on the voltages that excite the windings, in order to get ripple current steering, is that they are proportional, with the same frequency and phase
3. Provided the above condition on the terminal voltages is met, the zero-ripple current occurrence in one winding depends on a proper choice of the leakage inductance associated with the other winding only
4. As a winding where zero-ripple current occurs is virtually open for AC currents, the inductance seen at the terminals of the other winding is exactly equal to its self-inductance.

3 Sensitivity of zero-ripple current condition

In real-world coupled inductors it is unthinkable to reduce the ripple current in a winding to exactly zero and produce a perfect ripple steering. There are two basic reasons for this:

- Zero-ripple condition mismatch. In practice, the inductance of a winding is determined by the number of turns and the average permeability of the associated magnetic circuit. The turn ratio can assume only discrete values (ratio of two integer numbers) and it is difficult to control the average permeability to achieve the exact value that allows the meeting of the condition in *Equation 7* or any equivalent (*Equation 6*). Even if this may be obtained in occasional samples, manufacturing tolerances cause the actual value to deviate from the target in mass production
- Impressed voltage mismatch. In real operation, there are several factors that cause the two windings to be excited by voltages that are not exactly equal to one another, such as the voltage drop across the winding resistance (neglected so far), or the mere inability of the external circuit to do so. For example, in the smoothing transformer, the finite capacitance value of CS and its ESR cause an impressed voltage mismatch even in the case of ideal windings. To evaluate the residual ripple current it is convenient to use the a = k n_e model in *Appendix A*, already used (*Figure 4*) for deriving the zero-ripple current condition. Based on that, it is possible to write:

Equation 8

$$\frac{di_2(t)}{dt} = \frac{v_2(t) - k\, n_e v_1(t)}{L_2\left(1-k^2\right)}$$

which, after a simple algebraic manipulation, can be re-written as:

Equation 9

$$\frac{di_2(t)}{dt} = \frac{1}{L_2\left(1-k^2\right)}\left[\underbrace{v_2(t) - v_1(t)}_{\text{Impressed voltage mismatch}} + \underbrace{\left(1-k\, n_e\right)v_1(t)}_{\text{Zero ripple condition mismatch}}\right]$$

Although the inductance of the DC winding is theoretically irrelevant to the phenomenon itself (the inductance could even be zero), *Equation 7* and *8* show that this inductance is significant in practice, because it determines the actual residual ripple current resulting from the unavoidable aforementioned mismatches. More precisely, these equations highlight the need for a high-leakage magnetic structure, so that a low coupling coefficient k maximizes the “residual” inductance L_2 (1-k^2).

Note that a low value for k also means that the value of n_e that meets the zero-ripple condition is higher: for a given primary inductance L_1, this implies a higher value of L_2, and so further contributing to keeping the ripple low.

With the aim of assessing the amount of ripple attenuation in case of a non-ideal cancellation, considering an assigned value for L_1 is an important practical constraint. As previously stated, the inductor ripple current on the cancellation winding is just determined by its inductance L_1 and this ripple is seen by the power switch of the converter. This means that, if L_1 is unchanged, the converter circuit still operates exactly under the same conditions even with the use of the additional coupled inductor.

If the attenuation A is defined as the ratio of the residual ripple $di_2(t)/dt$, given by *Equation 7* or *8*, to the ripple that would be there without the coupled inductor ($di_1(t)/dt = v_1(t)/L_1$, equal to the actual ripple on the cancellation winding, as L_1 is unchanged), it is possible to write for the worst case scenario:

Equation 10

$$A = \frac{\frac{di_2(t)}{dt}}{\frac{di_1(t)}{dt}} = \frac{L_1}{v_1(t)}\frac{di_2(t)}{dt} = \rho\left(\left|\frac{\Delta v(t)}{v_1(t)}\right| + |\delta|\right)$$

where $\Delta v(t) = v_2(t) - v_1(t)$ is the absolute voltage mismatch, $\delta = k\, n_e - 1$ is the zero-ripple condition mismatch (absolute and relative values coincide) and the factor ρ is given by:

Equation 11

$$\rho = \frac{1}{(1+\delta)^2}\frac{k^2}{1-k^2}$$

In *Figure 7* the attenuation A is plotted for different values of the relative voltage mismatch $\Delta v(t)/v_1(t)$ and of the coupling coefficient k, as a function of the zero-ripple condition. From the inspection of these plots, it is apparent that a low coupling coefficient is essential for a good attenuation even if the zero-ripple condition is not exactly met. To achieve attenuations always greater than 10-12 dB even with a tolerance of ±10 % on the value of δ and 10 % voltage mismatch, the coupling coefficient k must be around 0.7. Lower k values would lead to a higher insensitivity of the zero-ripple condition due to mismatches but lead to more turns for the DC winding, which could become an issue in terms of inductor construction.

Note that in case of under-compensation ($\delta<0$) the residual ripple can be higher than the original value: this is due to a too low value of the “residual” inductance L_2 $(1-k^2)$.

Extending these concepts to the smoothing transformer of *Figure 3*, where the voltage externally applied to the AC winding is affected by the voltage ripple on the capacitor C_S (due to its finite capacitance value as well as its ESR), the voltage mismatch $\Delta v(t)/v_1(t)$ and, as a result, also the attenuation A, become frequency-dependent. Magnetic flux distribution modifications with frequency, which also affect δ, are a second-order effect and are neglected.

References 1 and *2* provide a complete analysis of the smoothing transformer frequency behavior. Here it is convenient only to summarize the results:

1. The smoothing transformer is capable of a third-order attenuation of current ripple, i.e. it is equivalent to an inductor combined with an additional LC filter
2. The transfer function generally includes three poles and two zeros; if the zero-ripple condition is fulfilled ($\delta=0$), the two zeros go to infinity and the smoothing transformer becomes a third-order all-pole filter
3. Modeling winding resistance and capacitor ESR produces a little damping of the pole-zero resonances but do not significantly affect the imaginary component of their locations
4. The effect of the zero-ripple condition mismatch ($\delta\neq0$) is to move the zero pair towards the poles, therefore creating some “notch” frequencies where greater attenuation is achieved, but degrading the overall attenuation produced at higher frequencies

Figure 7. Ripple-current attenuation as a function of the error sources for various winding coupling

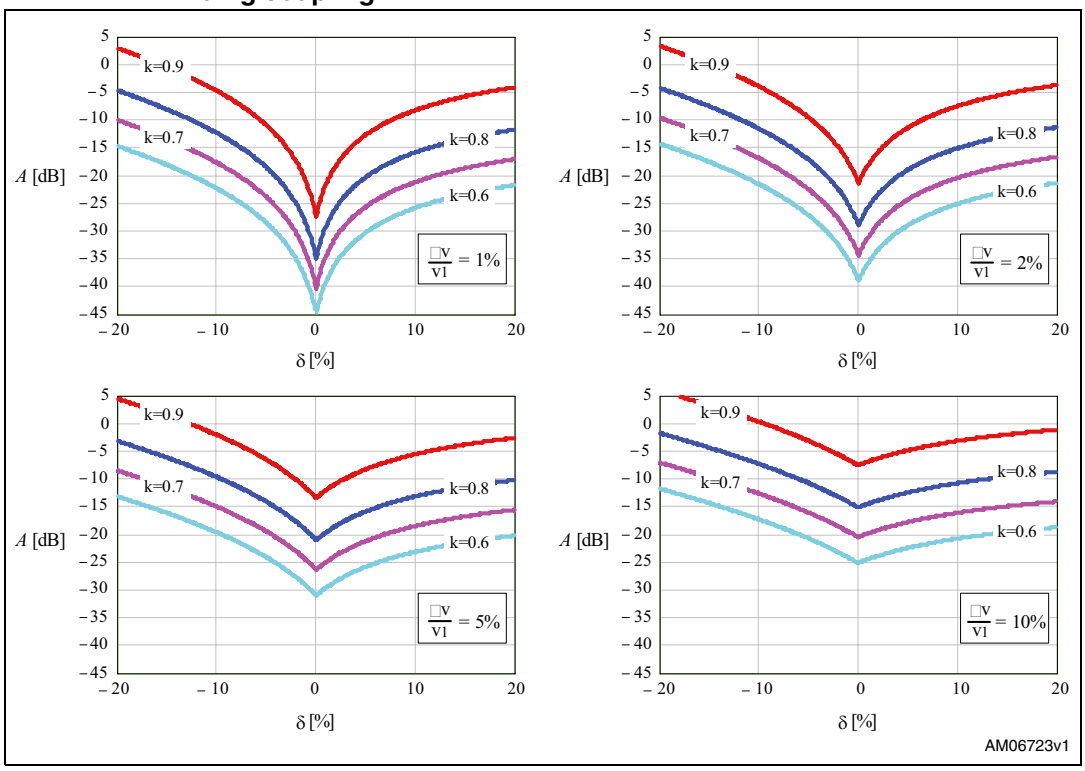

5. A resonance frequency, close to:

Equation 12

$$f_r = \frac{1}{2\pi\sqrt{L_1 C_S}}$$

for small zero-ripple condition mismatches, exists where the gain peaks and attenuation may be lost. However, the parasitic resistances damp this peak so that it is not high, even though its effect might be visible in the waveforms, should that frequency be stimulated; anyhow, to get the desired attenuation at the switching frequency and above, the practical values of C_S are such that the peak occurs at a much lower frequency, where EMC regulations do not generally apply.

4 Zero-ripple current phenomenon: practice

Before giving details of the practical realization of a coupled inductor able to provide ripple steering, it is useful to draw some conclusions of considerable practical interest from the theoretical analysis carried out in the previous sections:

1. The fundamental point is that to achieve zero-ripple current in a coupled inductor with low sensitivity to parameter spread, a high-leakage magnetic structure is needed, which is contrary to the traditional transformer design practice. Then, in the important case of inductors realized with a gapped ferrite core plus bobbin assembly, the usual concentric winding arrangement is not recommended, although higher leakage inductance values can be achieved by increasing the space between the windings. However, it is difficult to obtain a stable value, because it depends on parameters (such as winding surface irregularities or spacer thickness) which are difficult to control. Other methods are used, such as placing the windings on separate core legs (if using an EE core) or side-by-side on the same leg. The latter arrangement is possible with both EE and pot cores (see *Figure 8*). They permit much more stable leakage inductance values, because they are related to the geometry and the mechanical tolerances of the bobbin, which are much better controlled. At this point there is the practical issue of finding suitable bobbins for such arrangements: large production quantities could make the case for a custom product, but using something readily available in the market is a good choice anyway. Slotted bobbins, like those illustrated in *Figure 9*, are quite commonly available from several manufacturers; they easily lend themselves to a side-by-side winding arrangement, and they are considered here.

Figure 8. Examples of high-leakage magnetic structures (cross-section)

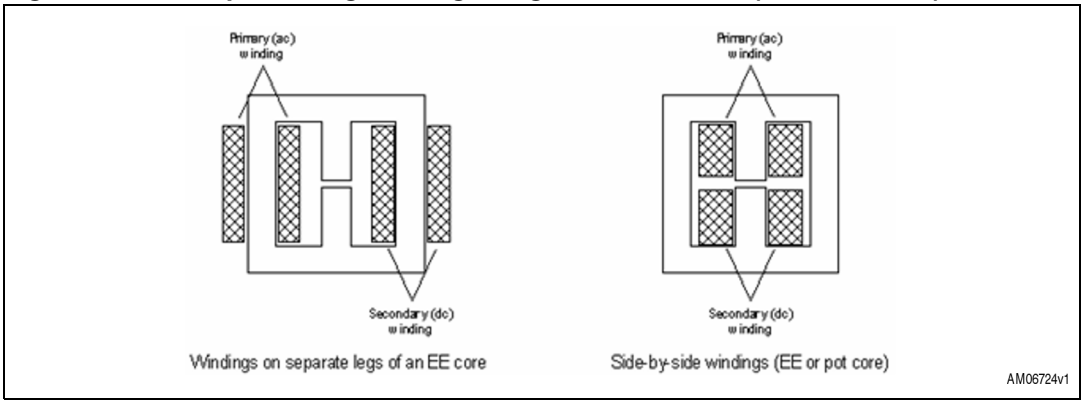

2. The fundamental action of the smoothing transformer is to split up the current into its DC component, which flows in the DC winding, and its AC component, which flows in the AC winding. In this way the total rms current in the windings is unchanged, hence the total copper area needed to handle the two currents separately is quite close to that of a single inductor carrying the total current. As compared to a single inductor, no core size increase is typically expected because of insufficient winding window area, except for a few marginal cases where the slight decrease of window area due to slotting becomes critical or where the DC winding has many more turns. It is also worth noting that the DC winding can be made with a single wire, as its residual AC current is low; only the AC winding is made with litz or multi-stranded wire. This minimizes the additional cost of the added winding.

Figure 9. Two-section slotted bobbin suggested for the realization of a coupled inductor - top view

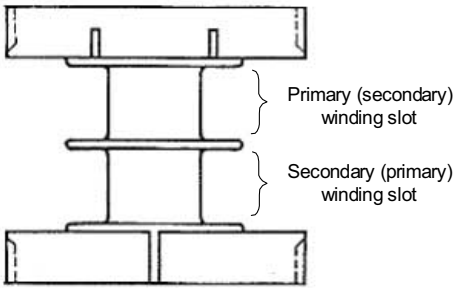

Figure 10. Two-section slotted bobbin suggested for the realization of a coupled inductor - side view

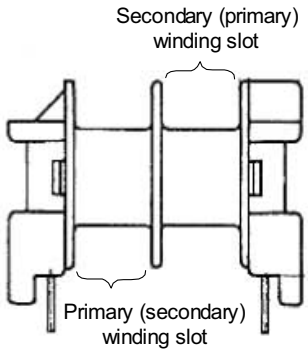

3. As a result of the aforementioned current splitting action, the same happens to the magnetic flux: the AC winding is responsible for generating the AC component of the flux and the DC winding for its DC component, but their sum is the same as in a single inductor carrying the total current. This means that no core size increase is expected because of flux density limitations (core saturation) or core loss reasons. Also the core size selection approach is the same.

To complete the picture, an important property of the “gapped ferrite core plus bobbin” assembly should be recalled. The reluctance of the leakage flux path is constant for a given core geometry and is independent of the gap thickness, l_{gap}: essentially, it is a function of the physical dimensions of the core and the distance between the windings. This implies that the leakage inductance of the primary winding, Ll1, depends only on the turn number N_1 and does not change if l_{gap} is adjusted. However, the total primary inductance $L_1 = L_{l1} + L_M$ is strongly affected by the gap thickness, but it is only the magnetizing inductance L_M that changes. With reference to the zero-ripple current condition in *Equation 7*:

Equation 13

$$\frac{L_M}{L_{\ell 1} + L_M} n = \frac{L_1 - L_{\ell 1}}{L_1} n = 1$$

once the ferrite core and the associated bobbin are defined, it is thereby possible to control LL_{l1} and L_M separately, acting on N_1 and l_{gap} respectively, then the secondary turn number N_2 is determined so that the ratio $n = N_2/N_1$ meets the condition in *Equation 7*.

At this point, all the elements needed to outline a step-by-step practical design procedure are in place. For the details of steps 2 to 4, please refer to the algorithm described in *References 3*.

1. The case of a conventional inductor is considered. From the circuit design determine the required inductance value L_1, the maximum peak short-circuit current and, considering full load conditions, the rms, DC and AC inductor currents, recalling that between them the following relationship holds:

Equation 14

$$I_{AC} = \sqrt{I_{RMS}^2 - I_{DC}^2}$$

In the case of a flyback transformer the winding to consider is the one on the side where the ripple current is to be cancelled. For the forward converter the inductor to consider is the output filter inductor.

2. Assuming that an EE-shaped ferrite core with a slotted bobbin is used, determine the maximum flux density and the maximum flux swing the core is operated at. Tentatively select a core size and determine the loss limit, both in the winding (P_{Cu}) and the core (P_{Fe}). Calculate the turn number N_1 of the AC winding in such a way that the desired inductance value L_1 can be obtained without exceeding either the core saturation limits or the permitted core losses. Determine the required gap length
3. Calculate the conductor size for the AC winding considering that its resistance must be:

Equation 15

$$R_{ac} \leq \frac{P_{Cu}}{I_{AC}^2}$$

To minimize skin and proximity effects, use litz or multi-stranded wire.

4. Calculate the conductor size for the DC winding considering that its resistance must be:

Equation 16

$$R_{dc} \leq \frac{P_{Cu}}{I_{DC}^2}$$

As DC current flows through this winding a single wire is used.

5. Wind the entire AC winding in one slot and, in the other slot, wind a couple of layers of the wire which is used for the DC winding. Temporarily assemble the core set. If the two half-cores are not gapped, use a gap value close to that calculated, to make the measurements that follow under conditions as close to those of a finished sample as possible. Consider also that a small gap amplifies measurement errors
6. Using any of the methods described in *Appendix B*, measure the leakage inductance L_{Lk} (referred to the AC winding) obtained in this way and calculate a first-cut value for N_2:

Equation 17

$$N_2 = N_1 \frac{L}{L - L_{LK}}$$

where, in this case, L is the measured inductance of the AC winding. Add 5 % to the result, to account for the slight coupling improvement that there is as the DC winding is entirely in place, and round up to the next integer. Let this number be N_2

7. After removing the layer used for the preliminary measurement and the core, wind the N_2 turns of the DC winding. Do not permanently fix the end of the wire because N_2 should be greater than the value that meets the zero-ripple condition and some turns need to be taken out in the following step
8. Reassemble the core and adjust the air gap so as to get the required value L1. Measure the leakage and the magnetizing inductances (see *Appendix B*) and check if (7) is met. If not, remove one turn and repeat the step until the condition in *Equation 7* is close to being met
9. Connect the coupled inductor to the converter, power it on and measure the ripple on the DC winding. It should be quite small. If it looks like that in *Figure 11* the turn number of the DC winding has been reduced too much. If it is not possible to add more turns to the DC winding, either the air gap must be reduced, if possible (paying attention to saturation!), or the turns number of the AC winding must be reduced. If the ripple looks like that in *Figure 12*, where the ripple is 180° out-of-phase, there are still too many turns on the DC winding and they should be further reduced. Also in this case it is possible to fine tune by adjusting the gap, if possible. Only now can the DC winding wire end be permanently fixed to the bobbin pin. Record the final values of N_1, N_2 and l_{gap}.

Figure 11. Partial ripple cancellation: still under compensated

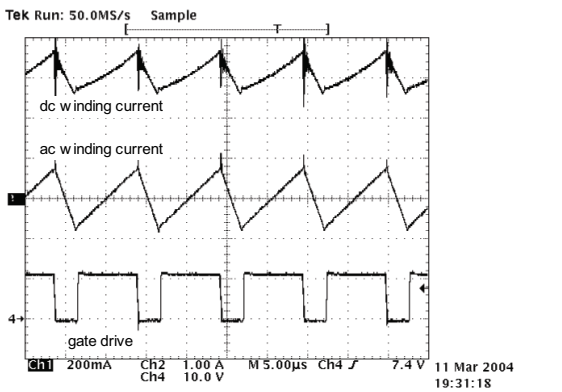

Undercompensated (kn_e <1):
dc winding with too few turns

AM06727v1

Figure 12. Partial ripple cancellation: overcompensated

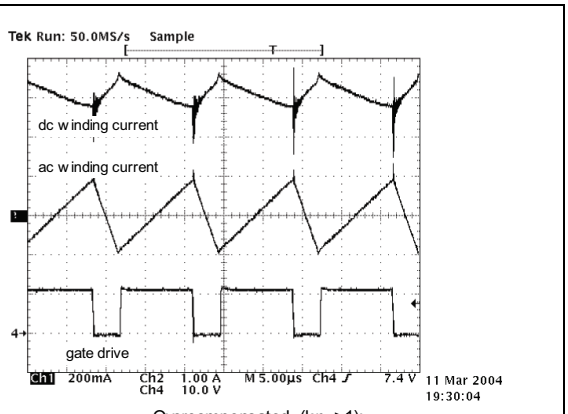

Overcompensated (kn_e >1):
dc winding with too many turns

AM06728v1

Note that the first four steps of this procedure are the same as those for a conventional inductor. Starting from step 5, the procedure becomes empirical and quite tricky and might also be time-consuming. Fortunately, this work needs to be carried out only for the first prototype.

There is still an important practical issue to consider. When the two half cores are assembled, even if they are kept together well, they are typically quite loose inside the

bobbin, unless mounting clips or gluing are used (quite impractical to use during the cut-and-try phase). The position of the core inside the bobbin, especially along the direction of the legs, is critical because it changes the position of the air gap with respect to the windings. Moving the core causes significant variations of the magnetizing inductance, therefore it is recommended to fix the cores in a stable position as close as possible to that of the finished sample before doing any inductance measurement or test on the converter circuit.

It is now important to determine how much spread can be expected in mass production. Side-by-side winding arrangements in slotted bobbins are quite commonly used when making common-mode chokes. For wires which are not too thin (say, above 0.2 mm) with a good winding machine it is not difficult to have a tolerance of around 4-5 % on the leakage inductance. As for the self-inductance of one winding, using gapped cores the tolerance on the AL factor (nH/turn^2), deducible from ferrite core catalogs, is 5 % or better for air gaps >0.1mm for small cores (e.g. an E30/15/7) and for air gaps >0.4 mm in case of bigger cores (e.g. an E55/28/21). An additional 3 % tolerance has to be typically considered due to the above mentioned displacement of the core inside the bobbin. It is therefore possible to assume 5 % tolerance for L_{l1} and 8 % tolerance on L_1.

Turn ratio *n* is not subject to production spread, the rounding error just introduces a fixed mismatch in the zero-ripple current condition. Again, using gapped cores, where the air gap cannot be adjusted to compensate for the mismatch, the rounding error is 0.5 turns, therefore the maximum absolute error that it introduces on *n* is $\leq 0.5/N_1$ and the maximum relative error is $(0.5/N_1)/n = 0.5/N_2$.

With some simple algebraic manipulations it is possible to find the relative error on the zero-ripple current condition in *Equation 7* due to the spread δ_{l1} and δ_1 of L_{l1} and L_1, respectively:

Equation 18

$$\delta = (n-1)\frac{\delta_1 - \delta_{\ell 1}}{1+\delta_1}$$

As *n* is slightly greater than 1 the effect of the spread of L_{l1} and L1 is attenuated. For example, with *n*=1.3, the resulting maximum spread is δ = -4.2 % to +3.6 %.

With good approximation, it is possible to consider that this tolerance band is centered on a value shifted by the rounding error. Referring to *Figure 7*, the attenuation factor A degrades more quickly for negative values, therefore it is better to round N_2 to the upper integer, to provide a “positive offset” to δ and be in a region where A changes less. Furthermore, if N_2=50 turns (rounded up), the rounding error is +1 %, so that the total tolerance band is -3.2 %, +4.6 %.

5 Capacitor selection

It is obvious that the capacitance of the smoothing transformer capacitor should be as large as possible and its ESR as low as possible to minimize the impressed voltage mismatch. Although this assertion is always true, the use in a PFC pre-regulator to minimize the input current ripple poses an important limitation to the capacitance value that can be used.

In *Figure 2* it is shown that in the zero-ripple input current configurations there is a DC path between the capacitor and the input port of the converter. This means that, at low frequency, the capacitor appears as if directly connected to the input rectifier bridge; therefore, in a PFC stage it adds to the capacitor normally placed just after the bridge and contributes to the increase in total harmonic distortion (THD) of the low-frequency line current as well as to lowering the power factor (PF).

Actually, the capacitor placed after the bridge can be reduced because of the ripple reduction caused by the smoothing transformer; but the value of the smoothing capacitor must, in any case, be selected trading off the filtering performance of the smoothing transformer against the need for a low THD of the line current. The peak-to-peak voltage ripple Δv appearing across the capacitor, which is essentially twice the voltage mismatch, is related to the AC ripple amplitude ΔI:

Equation 19

$$\Delta v_{pk-pk} = \frac{\Delta I}{8 f_{sw} C_s}$$

which is a maximum at the top of the sinusoid at minimum line voltage, where the amplitude of the AC current is maximum and the switching frequency is close to its minimum value. Substituting the values that can be derived by the PFC relationships [*4*], it is possible to find the following expression for the relative voltage mismatch:

Equation 20

$$\left.\frac{\Delta v(t)}{V_1(t)}\right|_{max} = \frac{L_1}{4 C_s}\left(\frac{Pin_{max}}{Vin_{min}^2}\right)^2 \frac{Vout}{Vout - \sqrt{2}\, Vin_{min}}$$

Typically, the values normally used for the capacitor after the bridge (5÷15 nF/W) lead to a good compromise. Polypropylene capacitors are recommended for their low ESR.

6 A 200 W ripple-free input current PFC pre-regulator

Figure 13 shows the electrical schematic of the EVL6563S-ZRC200 demonstration board, a 200 W zero-ripple-current PFC pre-regulator (see BOM in *Table 1*) based on the boost topology modified by adding the cancellation winding to the boost inductor and a capacitor, to make a smoothing transformer to minimize the input ripple. *Table 2* lists its electrical specifications, while *Table 3* gives the details of the boost inductor.

The design of the pre-regulator is carried out exactly in the same way as for a traditional stage. The coupled inductor, the crucial element of this application, is designed following the previously outlined procedure.

The controller chip used is the L6563S [*5*], suitable for implementing transition-mode-controlled PFC pre-regulators up to 250-300 W. Other notable semiconductor devices used are the STF12NM50N (a second generation MDmesh™ 0.38 /500 V N-channel MOSFET) and the STTH5L06 (a Turbo2 ultrafast diode, optimized for use in transition-mode PFC stages).

A prototype of the pre-regulator has been built and evaluated on the bench. The diagrams of *Figure 14*, *15* and *16* show its typical performance; *Figure 17* to *22* show some significant waveforms.

Figure 13. 200 W PFC pre-regulator with ripple-free input current: electrical schematic

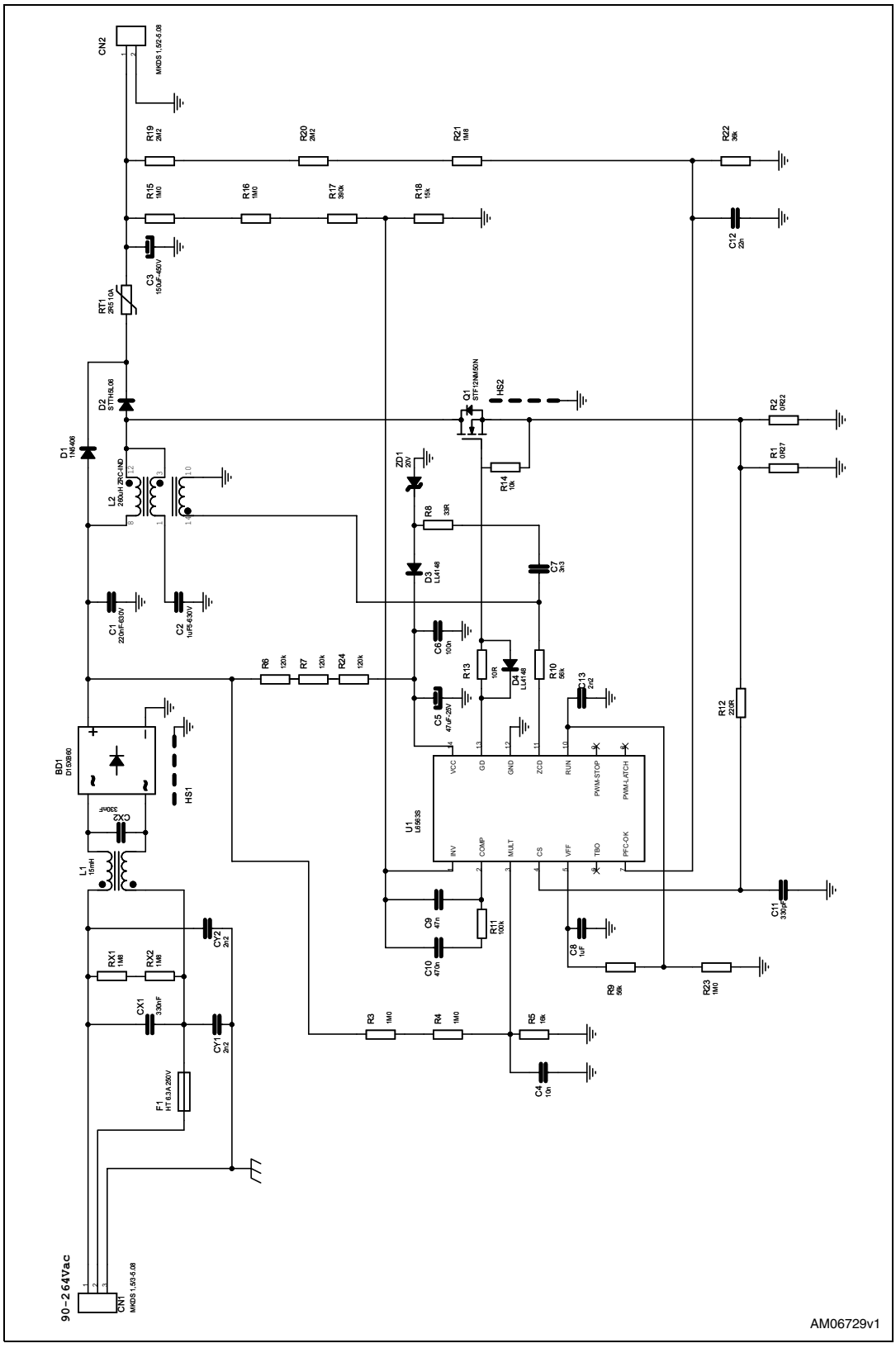

Table 1. Bill of material

Ref.	Value	Description	Supplier
BD1	D15XB60	15 A/600 V single phase bridge rectifier	SHINDENGEN
C1	220 nF-630 V	630 V polypropylene film capacitor	AVX
C2	1. 5 µF-630 V	630 V polypropylene film capacitor	EPCOS
C3	150 µF-450 V	450 V - aluminium ELCAP - MXG series - 105 °C	Rubycon
C4	10 *n*	SMD-0805 25 V CERCAP - general purpose	Murata
C5	47 µF-25 V	25 V - aluminium ELCAP - general purpose - 105 °C	NICHICON
C6	100 nF	SMD-0805 25 V CERCAP - general purpose	Murata
C7	3.3 nF	100 V CERCAP - general purpose	AVX
C8	1 µF	SMD-1206 16 V CERCAP - general purpose	Murata
C9	47 nF	SMD-0805 25 V CERCAP - general purpose	Murata
C10	470 nF	SMD-0805 16 V CERCAP - general purpose	Murata
C11	330 pF	SMD-1206 25 V CERCAP - general purpose	Murata
C12	22 nF	SMD-0805 25 V CERCAP - general purpose	Murata
C13	2.2 nF	SMD-0805 25 V CERCAP - general purpose	Murata
CX1	250 V 330 nF	X2 - safety CAP.	ARCOTRONICS
CX2	250 V 330 nF	X2 - safety CAP.	ARCOTRONICS
CY1	2.2 nF	Y1 - safety CAP - DE1E3KX222M	Murata
CY2	2.2 nF	Y1 - safety CAP - DE1E3KX222M	Murata
D1	1N5406	3 A/600 V rectifier-general purpose	STMicroelectronics
D2	STTH5L06	5 A/600 V high voltage ultrafast rectifier	STMicroelectronics
D3	LL4148	Fast switching diode	VISHAY
D4	LL4148	Fast switching diode	VISHAY
F1	FUSE 250 V 5 A	Fuse T5A - time delay	Wickmann
L1	15 mH	15 mH common mode choke	
L2	ZRC-IND-260 µH	ZRC-PFC inductor EC35 - PC44 (two slot bobbin)	
Q1	STF12NM50N	12 A/500 V N-channel power MOSFET	STMicroelectronics
R1	0.27 Ω	AXIAL stand. m-film res - 2 W -5 %	BC COMPONENTS
R2	0.22 Ω	AXIAL stand. m-film res - 2 W -5 %	BC COMPONENTS
R3	1.0 MΩ	SMD-0805 standard film res - 1/8 W - 1 % -100 ppm/°C	VISHAY
R4	1.0 MΩ	SMD-0805 standard film res - 1/8 W - 1 % -100 ppm/°C	VISHAY
R5	16 kΩ	SMD-0805 standard film res - 1/8 W - 1 % -100 ppm/°C	VISHAY
R6	120 kΩ	SMD-0805 standard film res - 1/8 W - 5 % -100 ppm/°C	VISHAY
R7	120 kΩ	SMD-0805 standard film res - 1/8 W - 5 % -100 ppm/°C	VISHAY
R8	33 Ω	SMD-0805 standard film res - 1/8 W - 1 % -100 ppm/°C	VISHAY

Table 1. Bill of material (continued)

Ref.	Value	Description	Supplier
R9	56 kΩ	Standard metal film res - 1/4 W - 1 % -100 ppm/°C	VISHAY
R10	56 kΩ	Standard metal film res - 1/4 W - 5 % -100 ppm/°C	VISHAY
R11	100 kΩ	SMD-0805 standard film res - 1/8 W - 5 % -100 ppm/°C	VISHAY
R12	220 Ω	Standard metal film res - 1/4 W - 5 % -100 ppm/°C	VISHAY
R13	10 Ω	SMD-0805 standard film res - 1/8 W - 5 % -100 ppm/°C	VISHAY
R14	10 kΩ	SMD-0805 standard film res - 1/8 W - 5 % -100 ppm/°C	VISHAY
R15	1.0 MΩ	SMD-0805 standard film res - 1/8 W - 1 % -100 ppm/°C	VISHAY
R16	1.0 Ω	SMD-0805 standard film res - 1/8 W - 1 % -100 ppm/°C	VISHAY
R17	390 kΩ	SMD-0805 standard film res - 1/8 W - 1 % -100 ppm/°C	VISHAY
R18	15 kΩ	SMD-0805 standard film res - 1/8 W - 1 % -100 ppm/°C	VISHAY
R19	2.2 MΩ	SMD-0805 standard film res - 1/8 W - 1 % -100 ppm/°C	VISHAY
R20	2.2 MΩ	SMD-0805 standard film res - 1/8 W - 1 % -100 ppm/°C	VISHAY
R21	1.8 MΩ	SMD-0805 standard film res - 1/8 W - 1 % -100 ppm/°C	VISHAY
R22	36 kΩ	SMD-0805 standard film res - 1/8 W - 1 % -100 ppm/°C	VISHAY
R23	1.0 MΩ	SMD-0805 standard film res - 1/8 W - 1 % -100 ppm/°C	VISHAY
R24	120 kΩ	SMD-0805 standard film res - 1/8 W - 5 % -100 ppm/°C	VISHAY
RT1	2.5 Ω 10 A	2.5R NTC resistor	EPCOS
RX1	1.8 MΩ	SMD standard film res - 1/4 W - 5 % - 250 ppm/°C	VISHAY
RX2	1.8 MΩ	SMD standard film res - 1/4 W - 5 % - 250 ppm/°C	VISHAY
U1	L6563S	Transition-mode PFC controller	STMicroelectronics

Table 2. 200 W PFC pre-regulator with ripple-free input current: electrical specification

Symbol	Description	Value	Unit
V_{ACmin} - V_{ACmax}	Line voltage range	90 - 265	Vrms
V_{out}	Regulated output voltage	400	Vdc
P_{out}	Rated output power	200	W
f_{swmin}	Minimum switching frequency	40	kHz
h	Expected minimum efficiency	90	%
ΔV_{out}	Full-load output voltage ripple	15	Vpk-pk
ΔV_{OVP}	Maximum output overvoltage	45	Vdc

Table 3. 200 W PFC pre-regulator with ripple-free input current: coupled inductor specification

Item	Description				
Core	2xEFD35, PC40 material grade				
Bobbin	2-slot, 14 pins, horizontal mounting				
Inductance	AC winding inductance (pin 3-1): 260 µH DC winding inductance (pin 12-8): 490 µH leakage inductance (pin 12-8 with pin 1-3 shorted): 255 µH				
Windings spec and build	Winding	Pin S/E	Wire	Turns	Notes
	AC	3/1	100 x 0.1 mm	46	Wound in slot 1
	DC	12/8	0.7 mm	64	Wound in slot 2
	aux	14/5	0.3 mm	7	Evenly spaced, on top of AC winding

Figure 14. Harmonic emissions and conformity to JEITA-MITI standards

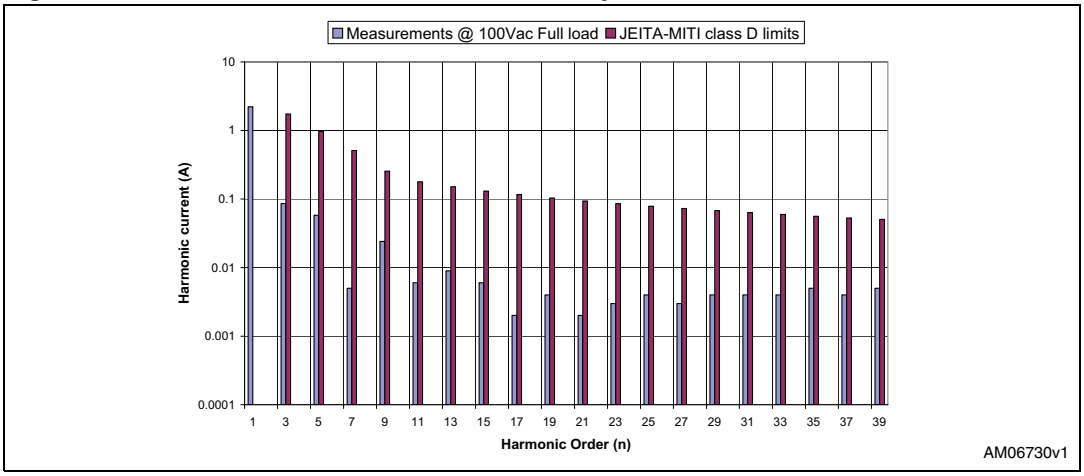

Figure 15. Harmonic emissions and conformity to EN61000-3-2 standards

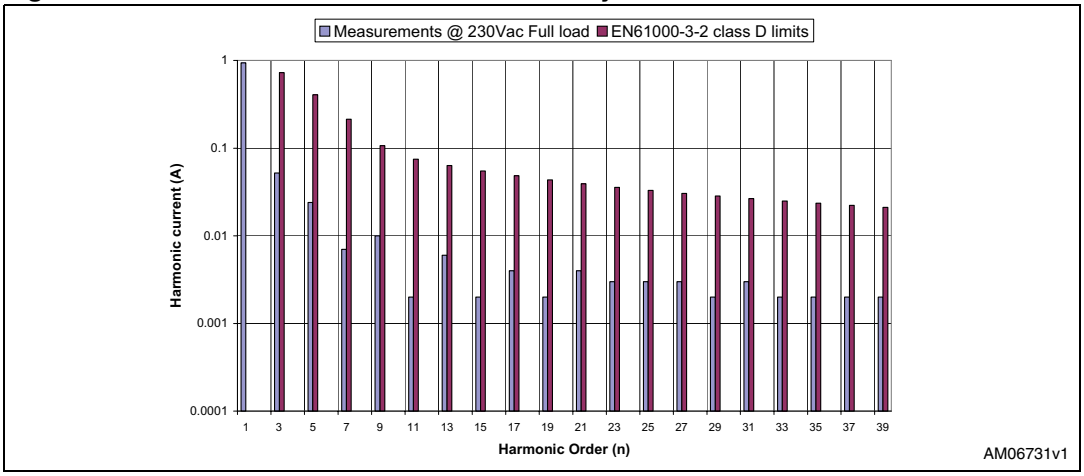

Figure 16. 200W PFC pre-regulator with ripple-free input current: typical performance

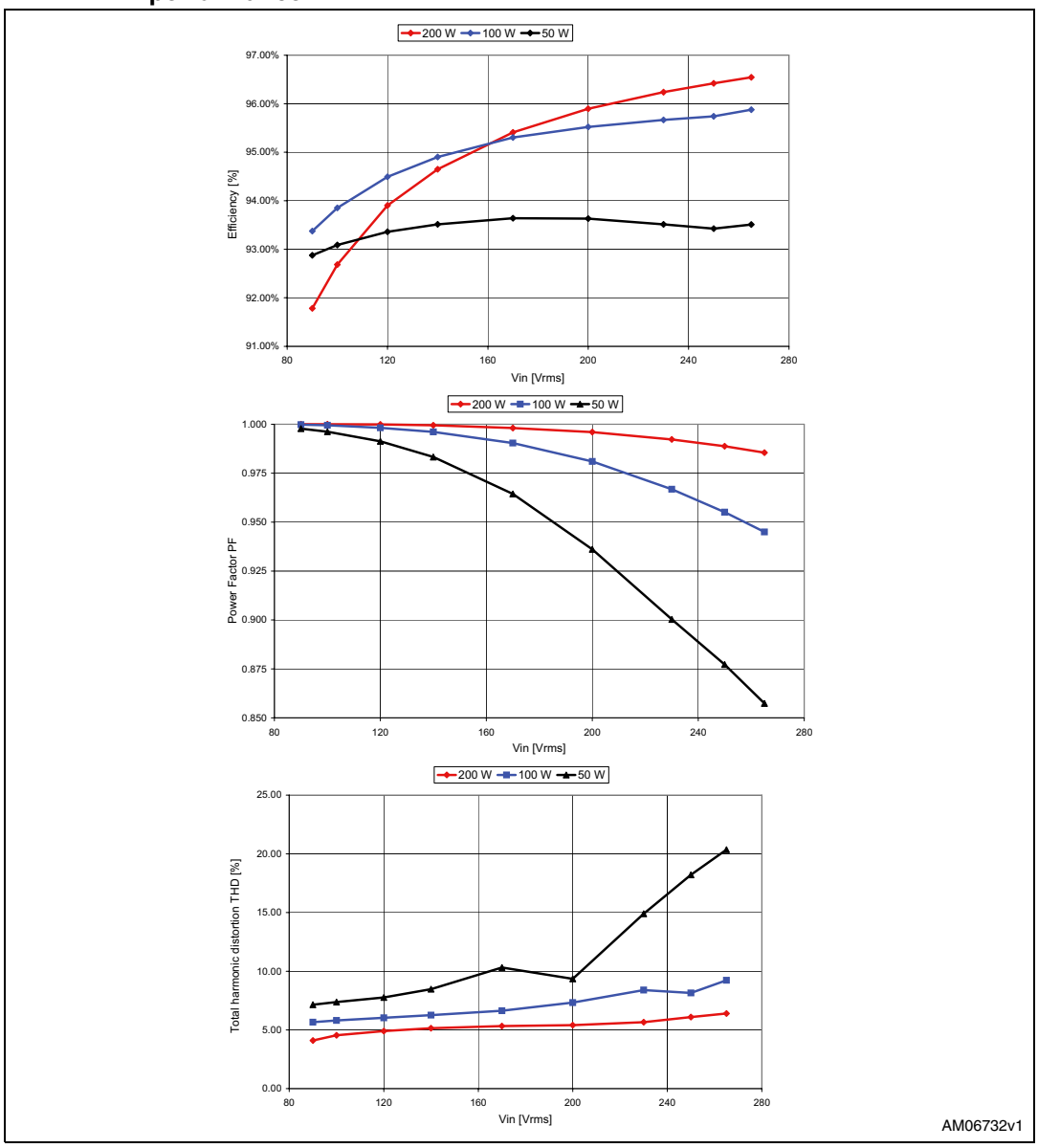

Figure 17. Line current and voltage @ full load (200 W) - Line current and voltage @ 115 Vac -200 W

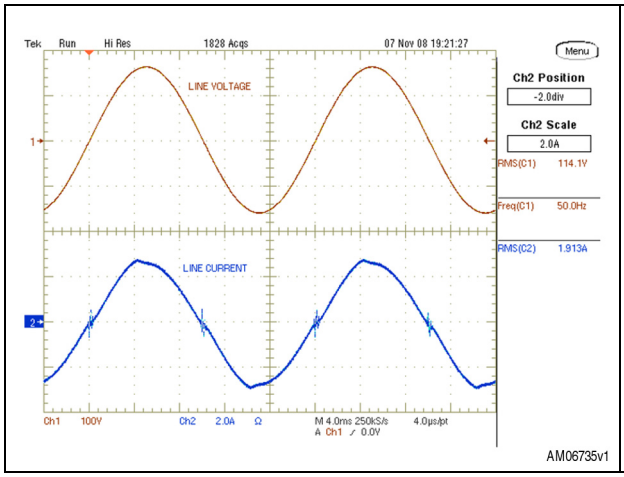

Figure 18. Line current and voltage @ full load (200 W) - Line current and voltage @ 230 Vac -200 W

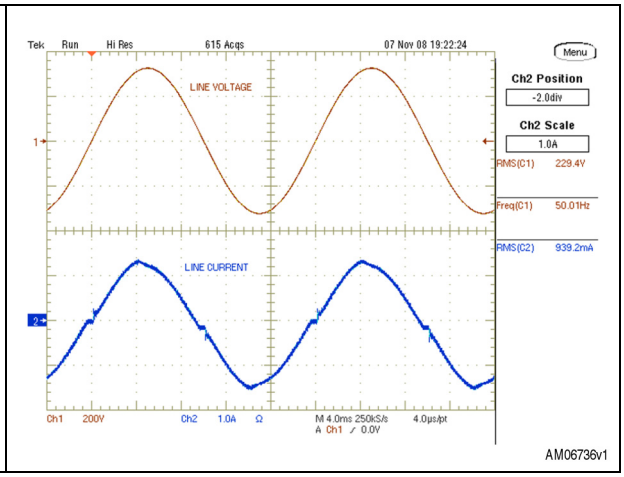

Figure 19. AC and DC winding currents nominal input voltages and full load (200 W) - AC and DC winding currents @ 115 Vac - 200 W

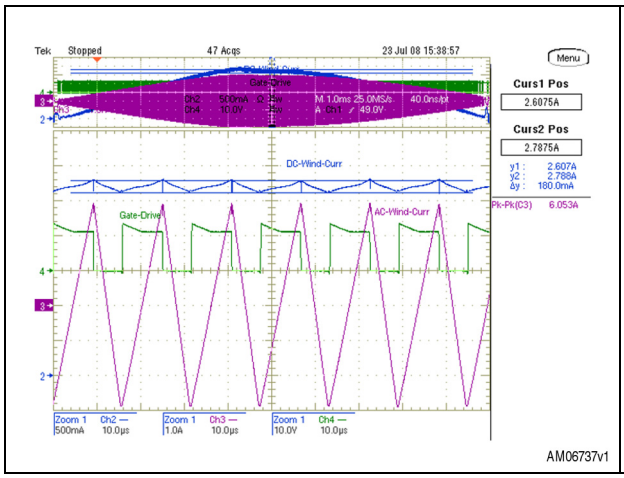

Figure 20. AC and DC winding currents nominal input voltages and full load (200 W) - AC and DC winding currents @ 230 Vac - 200 W

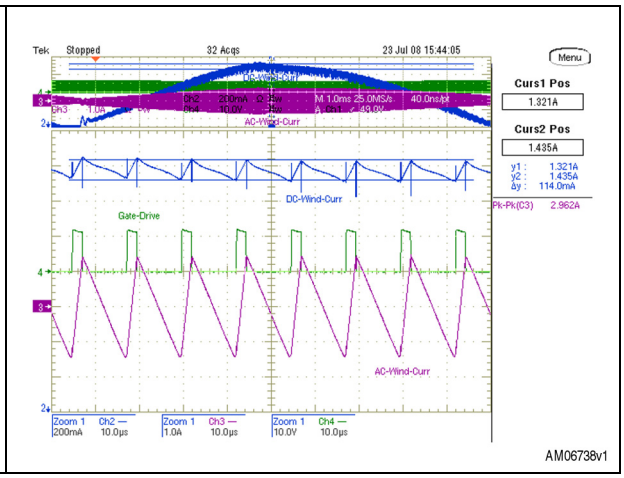

The waveforms of *Figure 17* to *20* are taken at full load. The images in *Figure 17* and *18* show the mains voltage and current drawn from the mains: this is quite sinusoidal, as in a standard transition mode PFC converter. In fact its harmonic content is well below the maximum allowed by current regulations (JEITA-MITI and European EN61000-3-2), as can be seen from *Figure 14* and *15*. Also the power factor and the total harmonic distortion parameters are as good as for a standard circuit without the cancellation winding, as can be seen from *Figure 16*, where also the efficiency measurements are plotted, showing values always greater than 91.7 %.

The zoomed image of *Figure 19* (@115 Vac) shows a residual ripple current in the DC winding of 180 mA pk-pk, against a 6.053 A pk-pk of the AC winding current (which would flow in the boost inductor in the conventional topology arrangement), and so resulting in 0.18/6.053 = 29.7*10-3 (-30.5 dB) attenuation.

The zoomed image of *Figure 20* shows a residual ripple current in the DC winding of 114 mA pk-pk, against a 2.962 A pk-pk of the AC winding current, and so resulting in 0.114/2.962 = 38.5*10-3 (-28.3 dB) attenuation.

The EMI filter used for reducing the line conducted interferences is a single cell filter made up of two X capacitors and a common mode inductor (see the electrical schematic in *Figure 13*: CX1, CX2, L1) and two further Y capacitors (CY1, CY2). In standard transition mode PFC converters (without the cancellation winding) a double cell filter is usually necessary to reduce the EMI emission to levels within the maximum allowed by current regulations. The effect of ripple steering is particularly conspicuous up to about 2 MHz, with more than 20 dB attenuation provided. For higher frequencies, where common mode noise is dominant, its effect becomes negligible and emissions must be controlled resorting to the usual noise control techniques. The EMI measurement results are shown in *Figure 21* and *22*: the emission level with peak detection is well below the quasi-peak and average limits envisaged by EN50022 class B.

Figure 21. Conducted EMI @ Vin = 110 Vac, Pout = 100 W. Limits: EN50022 class B - precompliance EMI test @ 115 Vac - 200 W

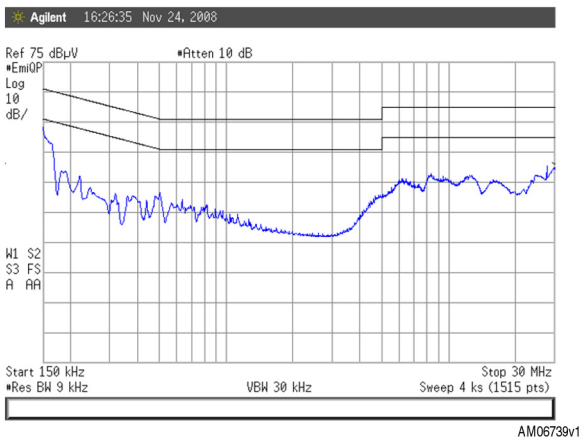

Figure 22. Conducted EMI @ Vin = 110 Vac, Pout = 100 W. Limits: EN50022 class B - precompliance EMI test @ 230 Vac - 200 W

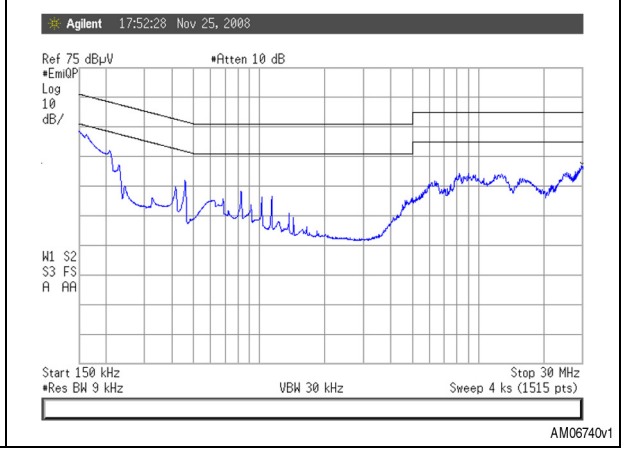

7 Conclusions

The ripple-steering technique, with its ability to reduce an inductor ripple current theoretically to zero, has been discussed and its theoretical base has been outlined. The construction of a coupled inductor is addressed and a practical design guide given to enable its successful implementation.

A practical application of the ripple-steering technique has been shown: it refers to a Transition-mode controlled PFC pre-regulator where the technique has been used to minimize the input ripple current, which is a major limitation to the use of this simple and efficient topology at higher power levels.

The experimental results have shown that the ripple-steering technique is very effective in reducing the input ripple current and that considerable savings can be achieved in the differential-mode input EMI filter, with the positive side effect of minimizing the loss due to the filter itself.

8 References

1. “A 'Zero' Ripple Technique Applicable to Any DC Converter”, Power Electronics Specialists Conference, 1999. PESC 99. 30th Annual IEEE (1999 Volume 2)
2. “The Coupled Inductor Filter: Analysis and Design for AC Systems”, IEEE Transactions on Power Electronics, Vol. 45, No. 4, August 1998, pp. 574-578
3. “Inductor and Flyback Transformer Design”, Unitrode Magnetics Design Handbook (MAG100A), Section 5
4. AN966; *L6561R, Enhanced transition mode Power Factor Corrector*, application note
5. L6563S; *Enhanced transition-mode PFC controller*, datasheet

Appendix A Electrical equivalent circuit models of coupled inductors and transformers

A system of coupled inductors is a set of coils that share one or more common magnetic paths because of their proximity. Because of this, magnetic flux changes in any one coil do not only induce a voltage across that coil by self-induction, but also across the others by mutual induction.

Accurate descriptions of coupled inductors use the reluctance model approach and its derivations, which closely represent the physical structure of the magnetic element. This approach is especially useful when dealing with complex magnetic structures, which is not the case under consideration. Here a simpler method is used based on the terminal equations describing the electrical behavior of the magnetic structure.

From an electrical standpoint, a system of m coupled inductors, is defined by m coefficients of self-inductance, relating the voltage across any inductor to the rate of change of current through the same inductor, and m·(m-1) coefficients of mutual inductance, equal in two by two, relating the voltage induced across any inductor to the rate of change of current in every other inductor.

Considering the important practical case of coupled inductors wound on the same core of magnetic material, each inductor is commonly termed “winding”. Focusing on the case m=2, a system of two coupled inductors, which are designated as the primary and the secondary winding, is a linear, time-independent two-port circuit described by the following branch-constitutive equations:

Equation 21

$$\begin{vmatrix} v_1(t) \\ v_2(t) \end{vmatrix} = \begin{vmatrix} L_1 & M \\ M & L_2 \end{vmatrix} \begin{vmatrix} \frac{d}{dt} \end{vmatrix} \begin{vmatrix} i_1(t) \\ i_2(t) \end{vmatrix}$$

where L1 and L2 are the self-inductances of the primary and the secondary windings respectively, and M is the mutual inductance. Winding resistance is assumed to be negligible.

Unlike L1 and L2, which are inherently positive, M can be either positive or negative, depending on the voltage polarity of the windings relative to one another: a positive rate of change of the current in one winding can induce a voltage either positive or negative in the other winding. As shown in *Figure 23*, this is indicated by dot notation, which follows three important rules:

1. Voltages induced in any winding due to mutual flux changes have the same polarity at dotted terminals
2. Positive currents flowing into the dotted terminals produce aiding magneto-motive forces
3. If one winding is open circuited and the current flowing into the dotted terminal of the other winding has a positive rate of change, the voltage induced in the open winding is positive at the dotted terminal.

Based on rule 1 and on the sign convention of the terminal voltages and currents of two-port circuits, it is easy to see that for the coupled inductors in *Figure 23* on the left M>0, while for those on the right M<0.

Figure 23. Coupled inductors

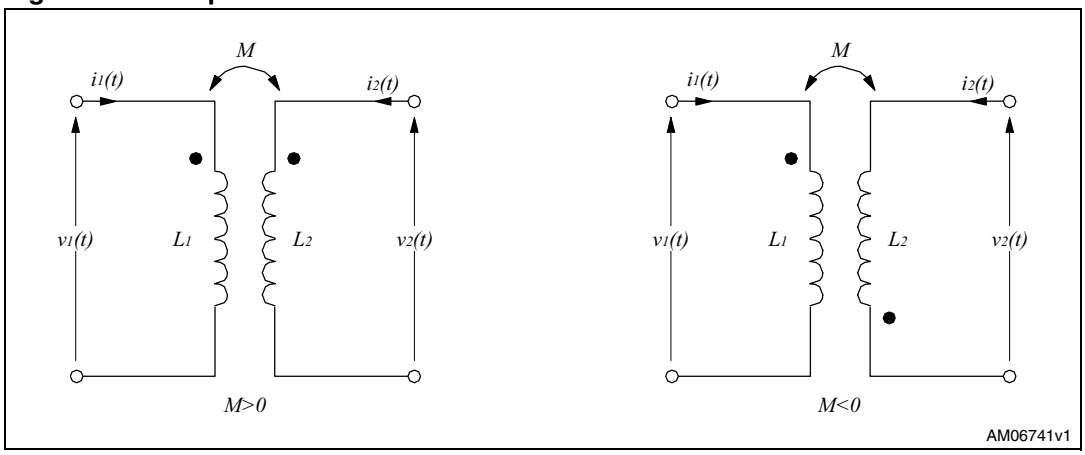

The mutual inductance M cannot be assigned arbitrarily but must fulfill the inequality:

Equation 22

$$|M| \leq \sqrt{L_1 L_2}$$

The case $|M| = \sqrt{L_1 L_2}$ is that of perfectly coupled inductors, that is when the magnetic flux generated by either winding is totally linked to the other. However, in real-world systems there is always some flux linking one winding but not the other or not completely linking the winding itself, e.g. because it “leaks” into the surrounding air; and so it is possible to write:

Equation 23

$$M = k\sqrt{L_1 L_2}$$

k, which lies in the range -1 k 1 is the so-called coupling coefficient and is a measure of the degree of magnetic coupling between the windings. For simplicity, from now on winding polarity is neglected and assume M>0 (and 0 k 1) always, the extension to the case M<0 being obvious.

It is possible to prove that k is the geometric mean of the portion k1 of flux generated by the first winding that links the second one, and the portion k2 of flux generated by the second winding that links the first one:

Equation 24

$$k = \sqrt{k_1 k_2}$$

Note that, in general, $k_1 \neq k_2$: fluxes do not necessarily link windings symmetrically one to another.

It is often useful to represent a system of coupled inductors with an equivalent circuit including an ideal transformer, that is a circuit element with a transfer function $v_2'(t) / v_1'(t)=a$ for voltages and $i_2'(t) / i_1'(t)= 1/a$ for currents. This equivalent circuit is shown in *Figure 24*.

Figure 24. Electrical equivalent circuit of coupled inductors

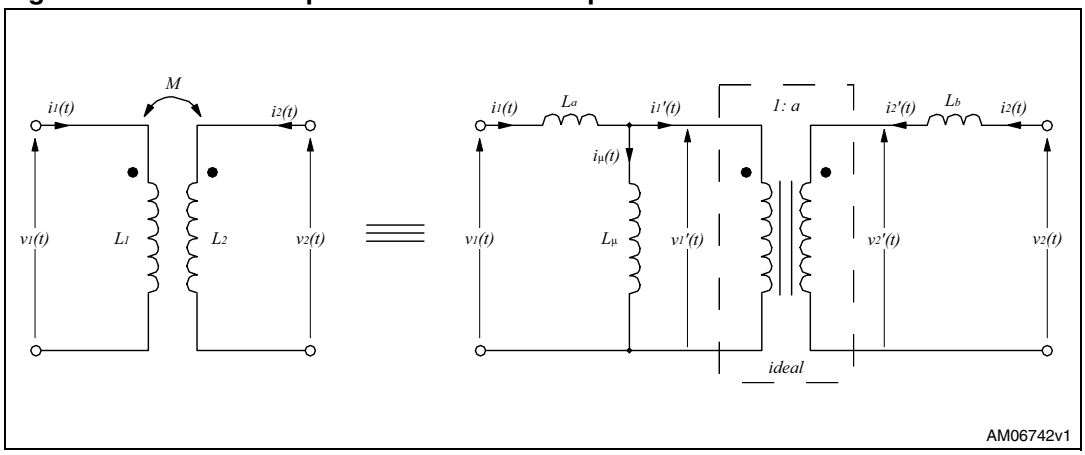

The branch-constitutive equations of the circuit are the following:

Equation 25

$$\begin{vmatrix} v_1(t) \\ v_2(t) \end{vmatrix} = \begin{vmatrix} L_\mu + L_a & a L_\mu \\ a L_\mu & a^2 L_\mu + L_b \end{vmatrix} \begin{vmatrix} \frac{d}{dt} i_1(t) \\ i_2(t) \end{vmatrix}$$

By comparing *Equation 25* to *21* it is possible to find the following relationships:

Equation 26

$$\begin{cases} L_1 = L_\mu + L_a \\ M = a L_\mu \\ L_2 = a^2 L_\mu + L_b \end{cases} \Rightarrow \begin{cases} L_a = L_1 - L_\mu \\ L_\mu = \frac{M}{a} \\ L_b = L_2 - a^2 L_\mu \end{cases} \Rightarrow \begin{cases} L_a = L_1 - \frac{M}{a} \\ L_\mu = \frac{M}{a} \\ L_b = L_2 - aM \end{cases}$$

It is important to notice that the model (*Equation 25*) and the resulting relationships (*Equation 26*) use four parameters (L_μ, L_a, L_b, a), but equations (*Equation 21*) show that three parameters only (L_1, L_2, M) are needed to completely define the two-port circuit. This means that one of the four parameters in (*Equation 25*) - a is the obvious choice - can be arbitrarily fixed, therefore leading to an infinite number of models (*Equation 25*) equivalent to (*Equation 21*).

A good criterion for choosing a is that both L_a and L_b have a positive value: should they result otherwise, the terminal equations would still be represented correctly but a negative inductance does not make physical sense and leads to wrong results as far as energy considerations are concerned.

It is possible to show that, if a equals the secondary-to-primary turns ratio n=N_2/N_1, L_a and L_b are always positive. Moreover, it is possible to prove that this choice leads to the same model as the reluctance model approach; and so the model with a = n is the physical model of a coupled inductor.

L_μ is associated to the mutual flux that links the primary and secondary winding mostly through the magnetic core, it is called primary magnetizing inductance and is designated by L_M; L_a is associated to the flux generated by the primary winding and not completely linked to itself or to the secondary winding, that is the primary leakage flux: L_a is therefore called primary leakage inductance and is designated by L_{l1}. Similarly, on the secondary side the

inductance L_b is associated to the secondary leakage flux, the flux generated by the secondary winding and not completely linked to itself nor to the primary winding: it is called secondary leakage inductance and is designated by L_{l2}.

This choice of a is perhaps the most logical one, and is also very useful because it provides a clear physical meaning to each element of the equivalent circuit, shown in *Figure 25*, but it is not the only one that makes sense.

Figure 25. Model of coupled inductors with a = *n* (a=*n* model)

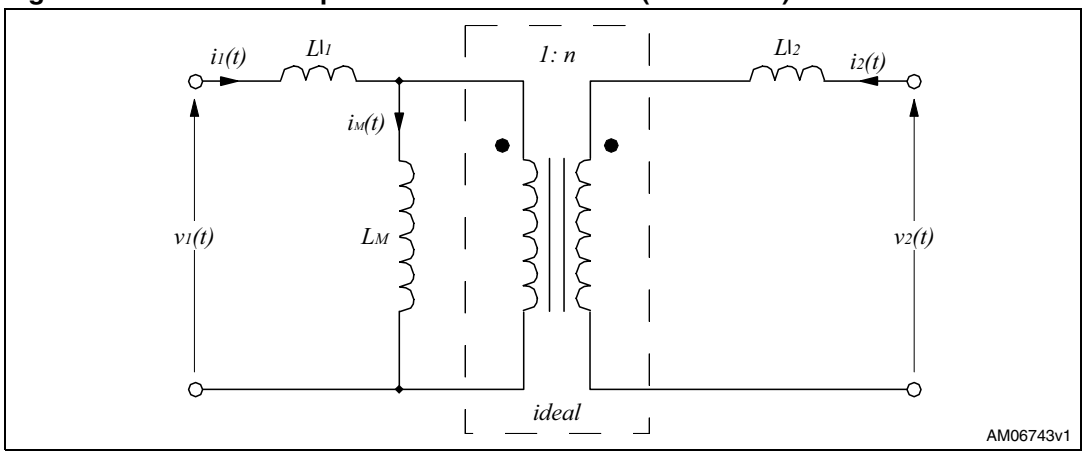

Another possible choice, which leads to always positive values for L_a and L_b, is a = $\sqrt{L_2/L_1}$. This quantity, usually indicated with n_e, is termed “equivalent turn ratio” and is conceptually and numerically different from the physical turn ratio *n*:

Equation 27

$$n_e = \sqrt{\frac{L_2}{L_1}} = \sqrt{\frac{L_{\ell 2} + n^2 L_M}{L_{\ell 1} + L_M}}$$

which coincides with *n* if and only if $L_{l2} = n^2 L_{l1}$, that is in case of symmetrical magnetic coupling ($k_1 = k_2 = k$).

This choice is particularly useful when the physical turn ratio *n* is unknown, so that it is possible to complete the model computing n_e from L_1 and L_2, which are easily measurable. In this case, *Equation 26*, considering *Equation 23*, takes the form:

Equation 28

$$\begin{cases} L_a = (1-k)L_1 \\ L_\mu = k\,L_1 \\ L_b = (1-k)L_2 = n_e^2\,L_a \end{cases}$$

It is worth noting that L_b, reflected back to the primary side, equals L_a, as pointed out by the third *Equation 28*. Note that this property is often erroneously attributed to the primary and secondary leakage inductances L_{l1} and L_{l2}. It is worth stating once more that k represents an average coupling between the windings and that the coupling k_1 of the primary winding to the secondary one is generally different from the coupling k_2 of the secondary winding to the primary one, and so $L_{l2} \neq n2\ L_{l1}$. It is $L_{l2} = n2\ L_{l1}$ only in the special case of a winding geometry symmetrical in such a way that the reluctance of the leakage flux path is the same for both windings, resulting in symmetrical coupling between windings ($k_1 = k_2 = k$).

Figure 26. Model of coupled inductors with a = n_e (a = n_e model)

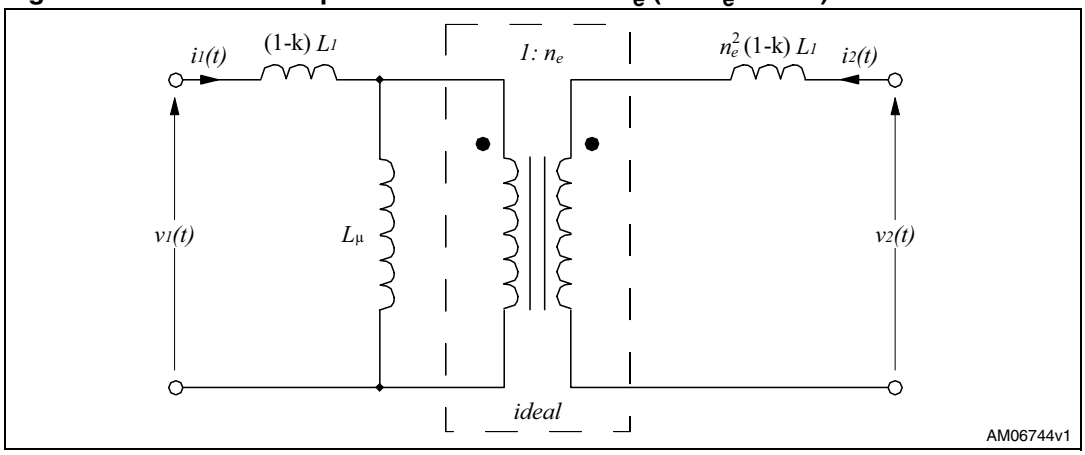

Another interesting and quite frequently used choice is a = 1. This results in a very simple model, illustrated in *Figure 27*, useful for analyzing loosely coupled inductors, where L_1-M and L_2-M are both positive, which happens if:

Equation 29

$$k < \min\left(\sqrt{\frac{L_1}{L_2}}, \sqrt{\frac{L_2}{L_1}}\right) = \min\left(\frac{1}{n_e}, n_e\right)$$

Note that the terminal voltages and currents are still exactly the same as those of the real inductors.

Figure 27. Model of coupled inductors with a = 1 (a =1 model, or T-model)

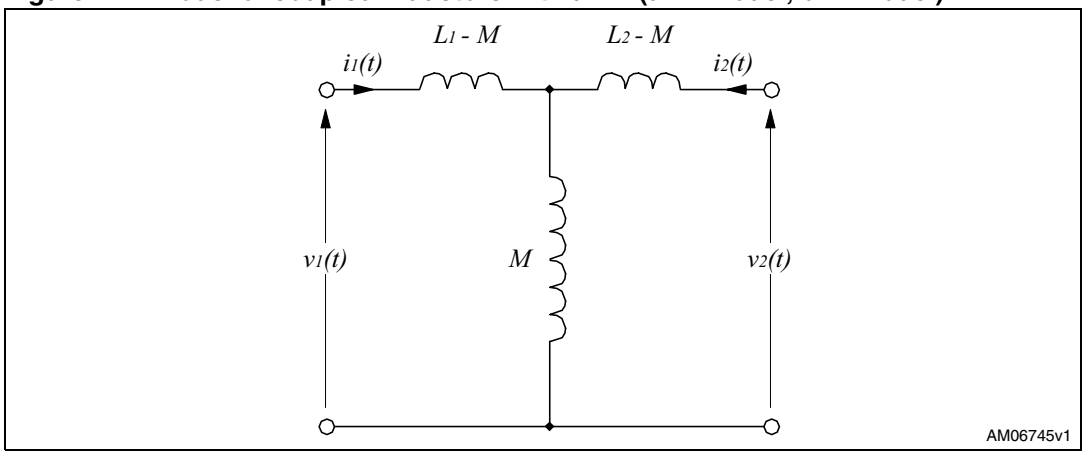

Figure 28. Model of coupled inductors with a = k n_e (a = k n_e model)

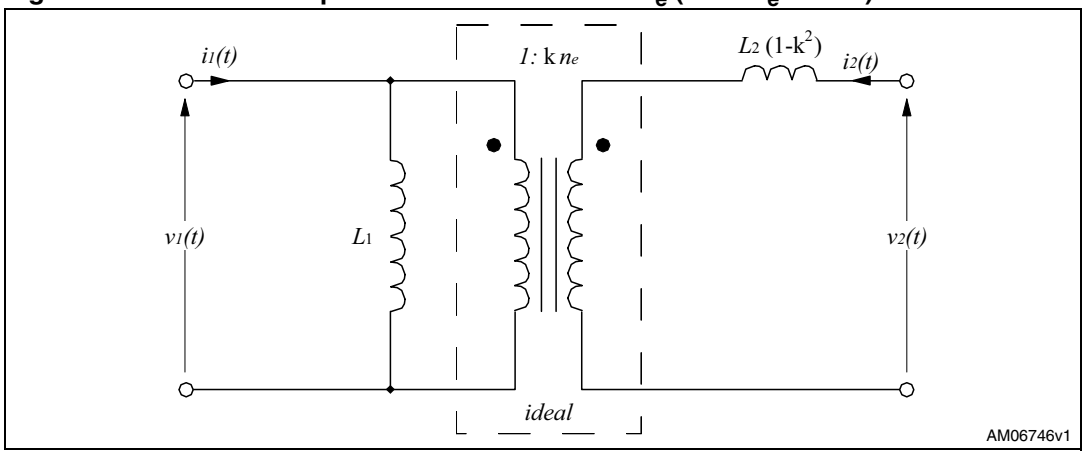

Other possible choices of a are a = M/L_1 = k n_e, which nulls L_a and puts all the elements related (logically, not physically) to the leakage flux on the secondary side (see *Figure 28*) and a = L_2 /M = n_e/k, which nulls L_b and puts all the elements related to the leakage flux on the primary side (see *Figure 29*).

From inspection of *Figure 28* and *29* it is apparent that the quantity L_2 (1-k^2) is the inductance of the secondary winding measured with a shorted primary winding and that L_1 (1-k^2) is the inductance of the primary winding with the secondary shorted out.

Figure 29. Model of coupled inductors with a = n_e/k (a = n_e/k model)

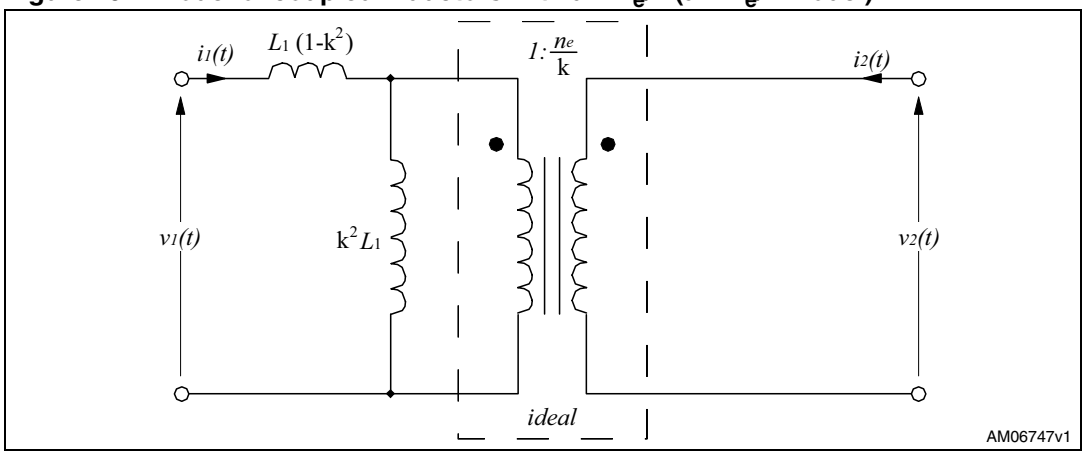

The usefulness of having different models available, dependent on the value attributed to a, is that it is possible to choose the one that best fits the specific problem under consideration, leading to a simpler solution or minimum mathematical manipulations.

An important assumption underlying the modeling techniques so far described, is that the behavior of the magnetic circuit, represented by an equivalent linear electric circuit, is also linear; that is, the magnetic flux is proportional to the magneto-motive forces that excite the windings. This is true only if the flux density inside the core is well below the saturation limit of the material.

The models can give useful information also on what happens in case the magnetic core saturates. With reference to the “physical model” of *Figure 25*, the leakage inductances L_{l1} and L_{l2} are relevant to magnetic flux that is located mostly in air and so they do not saturate and their value can be considered constant; the non linear element of the circuit is L_M, which

is associated to the magnetic flux that flows mostly through the magnetic core and so, is affected by the non-linearity typical of magnetic materials. If the flux density exceeds the saturation level, the permeability of the magnetic material μ drops dramatically almost to the free space value μ0; as a result L_M tends to be a much lower value and shunts the ideal transformer, so that, essentially, only L_{l1} and L_{l2} are visible from the terminals. Moreover, the windings are nearly decoupled and energy transfer is extremely low.

Finally, although transformers and coupled inductors work in a substantially different way (coupled inductors store energy, transformers ideally do not; in coupled inductors the magnetizing current - $i(t)$ in *Figure 24* - is directly related to the winding currents $i_1(t)$ and $i_2(t)$, in transformers it is related to the winding voltages $v_1(t)$ and $v_2(t)$ and to time, and this difference reflects also in the core saturation mechanism), they may be described by the same equivalent circuits. Therefore, the basic model of *Figure 24* and its derivatives of *Figure 25* to *Figure 29* can be indifferently considered as both coupled inductor models and transformer models.

Appendix B Measuring transformer and coupled inductor parameters

From a practical point of view there is the need to measure the parameters of coupled inductors (transformers) L_1, L_2 and M or, equivalently, k, and derive those of the equivalent circuits. Needless to say that it is of particular interest to obtain the parameters of the "physical model" with a = *n*, L_M, L_{l1} and L_{l2}.

L_1 and L_2 are directly measurable. To determine M or k appropriate measurements need to be done. The best way to proceed is to use a Z-meter, taking the measurements at a low enough frequency that the parasitic capacitance of the windings can be neglected. There are two basic methods to completely characterize a coupled inductor or a transformer from the electrical point of view: the open/short-circuit inductance (OS) method and the series-aiding/opposing inductance (AO) method.

According to the OS method, three measurements are taken:

- The primary inductance with the secondary open (L_1)
- The primary inductance with the secondary shorted (L_{1s})
- The secondary inductance with the primary open (L_2).

Through inspection of *Figure 29* it is very easy to derive the coupling coefficient from the L_{1s} measurement:

Equation 30

$$L_{1s} = L_1\left(1-k^2\right) \quad \Rightarrow \quad k = \sqrt{1-\frac{L_{1s}}{L_1}}$$

M is determined using (A2):

Equation 31

$$M = k\sqrt{L_1 L_2}$$

Measuring L_{1s} accurately might be an issue, and so this method is suitable when k is close to unity. It is not recommended when the winding resistance is not negligible.

The AO method is based on the fact that by connecting the two windings in series their combined inductance is given by $L_1 + L_2 \pm 2M$, where the sign given to 2M depends on the way the windings are connected, as shown in *Figure 30*. The difference of the two values is thereby equal to 4M.

According to the AO method, four measurements are taken:

- The primary inductance with the secondary open (L_1)
- The secondary inductance with the primary open (L_2)
- The combined inductance with series-aiding connection (L_A)
- The combined inductance with series-opposing connection (L_O).

Figure 30. Winding connections: aiding flux (left), opposing flux (right)

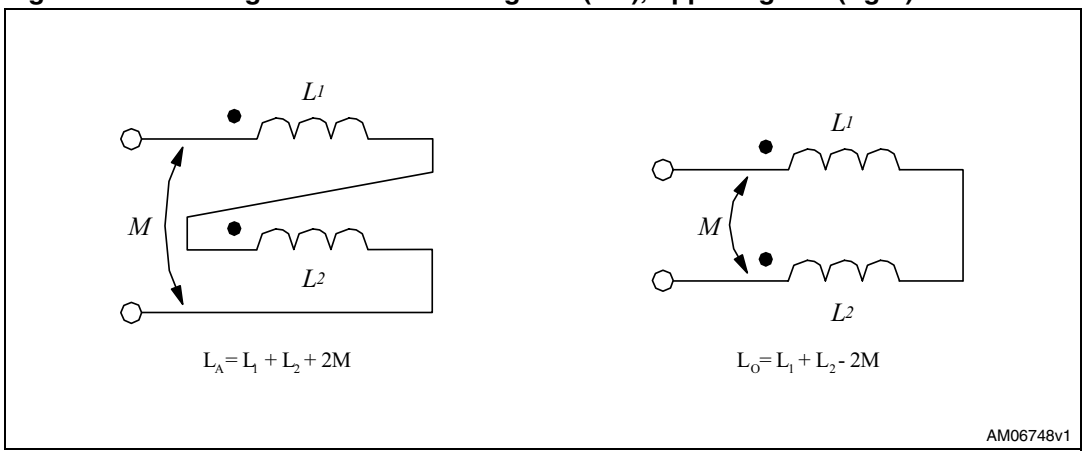

It is always $L_A > L_O$, therefore, as already mentioned:

Equation 32

$$M = \frac{L_A - L_O}{4} \quad \Rightarrow \quad k = \frac{L_A - L_O}{4\sqrt{L_1 L_2}}$$

The advantage of this method is its low sensitivity to winding resistance and to the impedance of the wire used for connecting the windings. It is not recommended for low values of k because in that case it would be given by the difference of two similar quantities, and the error might be high.

Whichever method has been used, the parameters of the equivalent circuit of *Figure 25* (a = *n*, assuming *n* is known) can be readily calculated from the third group of *Figure 26* with obvious symbolism change:

Equation 33

$$\begin{cases} L_M = \dfrac{M}{n} \\ L_{\ell 1} = L_1 - L_M = L_1 - \dfrac{M}{n} \\ L_{\ell 2} = L_2 - n^2 L_M = L_2 - nM \end{cases}$$

The parameters of the equivalent circuit of *Figure 26* (a = n_e, useful in case *n* is not known) are given by *Figure 28*, here re-written for convenience:

Equation 34

$$\begin{cases} L_a = (1-k)L_1 \\ L_\mu = k\,L_1 \\ L_b = (1-k)L_2 \end{cases}, \quad \text{with } n_e = \sqrt{\frac{L_2}{L_1}}$$

Revision history

Table 4. Document revision history

Date	Revision	Changes
14-Sep-2010	1	Initial release.